ORIGINAL RESEARCH ARTICLE

Atomic Ordering and Interfacial Interaction at Liquid-Mg/SiC{0 0 0 1} Interfaces: An *Ab Initio* Molecular Dynamics Study

CHANGMING FANG and ZHONGYUN FAN

We present the results of *ab initio* molecular dynamics investigations on the atomic ordering and chemical interactions at the interfaces between liquid Mg and SiC{0 0 0 1} interfaces. The simulations reveal distinct borders between the SiC substrates and liquid Mg. The liquid Mg atoms adjacent to the substrates are bonded to the outmost C/Si atoms and are positively charged. The terminating Mg layers contain a variety of atomic vacancies, being topologically rough. The liquid Mg atoms adjacent to the substrates display unusual prenucleation phenomenon with strong layering but weak in-plane ordering. The obtained information here is helpful to get insight into the formation and interfacial interactions in the SiC joined nano-sized magnesium matrix composites and the role of SiC particles as potential nucleation sites during solidification, and further helps understand interfacial interactions at the grain boundaries in ceramic/metal composites and welded parts, *etc*. in general.

https://doi.org/10.1007/s11661-023-07059-z

I. INTRODUCTION

MG metals have unique performances, including low specific weight (one-fifth of that of iron), high specific strengths and good castability.[1–3] Thus, Mg metals have been applied in various engineering fields, particularly for electronics, automotive and aerospace industries.[2,4] Advance in these industries demands more excellent mechanical performances of Mg metals. The hexagonal lattice of magnesium[3,5] indicates that the metals are weak in ductility.[2,4] Moreover, fine and uniform microstructures in the cast parts are desirable to improve their mechanical performances as shown in the recent studies[4] and in the reviews.[6,7]

One approach to improve the mechanical performances of the cast Mg metals is to add ceramics materials, such as SiC particles into Mg for the formation of nano-sized magnesium matrix composites (nano-MMCs).[6,8,9] Recently, Chen *et al*. realized a dense and uniform dispersion of SiC nanoparticles (14 vol pct) in Mg metals.[10] The obtained nano-MMC samples exhibit enhanced strength, high stiffness, excellent plasticity and high-temperature stability. Moreover, the added nano-sized SiC particles can act as potential nucleation sites during casting.[11–13] Knowledge about the atomic ordering and interfacial chemical interactions at the liquid Mg and SiC interfaces is therefore, essential for improving understanding about the role of the SiC particles in liquid Mg during casting and for designing new nano-MMCs of fine and uniform microstructures and desirable properties.

Above its nucleation temperature atomic ordering in the liquid adjacent to a solid-substrate is referred to as prenucleation.[14,15] Prenucleation provides a precursor for following nucleation and is crucial for the solidification.[16,17]

SiC has a hexagonal lattice.[5] Along its [0 0 0 1] axis the structure is composed of SiC double-atom layers. Each atom is tetrahedrally coordinated by the other species: three in the double-atom layer and one to the neighboring layer. Thus, both Si and C atoms satisfy the sp^3 bonding. Its crystal structure depends on stacking of the SiC double-atom layers. This makes SiC be unusually rich in polytypes (over 200 polytypes reported in the literature).[18–20] Among the polytypes, 4H- and 6H-SiC are prepared frequently. The unusual SiC structural feature indicates that it is reasonable to separate them between the SiC double-atom layers to create SiC{0 0 0 1} substrate-surfaces. The obtained SiC{0 0 0 1} surface is terminated either by C or by Si. Chemically, the difference of electronegativity between Si (1.90 in Pauling scale) and C (2.55) indicates polarity of the SiC{0 0 0 1} surfaces and the cleaved surfaces are thus, unstable at ambient conditions.[21] On one hand, it is different in (liquid) metals since the free electrons of the metal atoms compensate the polarity of the

CHANGMING FANG, and ZHONGYUN FAN are with the Brunel Centre for Advanced Solidification Technology (BCAST), Brunel University London, Uxbridge, UB8 3PH UK. Contact e-mail: changming.fang@brunel.ac.uk

Manuscript submitted February 6, 2023; accepted April 6, 2023.
Article published online April 27, 2023

substrate-surfaces.[22,23] On the other hand, the orientational sp^3 bonding nature of the Si and C atoms would have influences on the atomic ordering at the interfaces between the metal and the polar substrates.

There have been many experimental efforts about the MMCs and the crystalline-Mg/SiC interfaces. Experimental observations showed that contents of both Si and Mg have impact on the stability of SiC at high-temperature. There is a 'working zone' (temperature, Si-content, Mg-content) in the SiC/Mg–Si–Al system.[24] Experiments have focused on preparation,[12,25,26] structural characterization and improvements of mechanical performance of the produced (nano-)MMCs.[6–8,10,12] High-resolution electron microscopy techniques have been employed to investigate the local structures near the Mg/SiC interfaces of prepared samples and the orientational relations between SiC and Mg.[10,11,13,27] The SiC particles in the samples are dominated by the {0 0 0 1} facets.

Theoretical methods, epically parameter-free first-principles approaches have been employed to investigate the stability of the SiC polytypes,[28] their surfaces,[29] and interfaces between SiC and metals, dominantly Al[30] using the 6H-SiC,[31] 4H-SiC[32,33] and 3C-SiC[34,35] as substrates. Till now there is a dearth of knowledge on the interfaces between liquid Mg and SiC.

We here investigate the prenucleation at the liquid magnesium and SiC{0 0 0 1} (denoted as Mg(*l*)/SiC{0 0 0 1}) interfaces using an *ab initio* molecular dynamics (AIMD) technique. We observed distinct interfaces between the substrates and the liquid. There is strong layering but weak in-plane ordering in the liquid Mg adjacent to the substrates. This study also shows complex chemical bonding at the Mg(*l*)/SiC{0 0 0 1} interfaces. The obtained information here is useful to get insight into the chemical bonding in nano-MMCs, the role of the polar SiC substrates during casting, and further to design new nano-MMCs of fine and uniform microstructure and desirable properties.

II. DETAILS OF SIMULATIONS

To satisfy the periodic boundary conditions employed here, we built a hexagonal supercell containing SiC substrates and liquid-Al. The length of the in-plane *a*-axis is $a = 5\ a_0$, where a_0 is the length of the *a*-axis of the conventional hexagonal cell of 4H-SiC with consideration of the thermal expansion at the simulation temperature.[36] The length of the *c*-axis is determined by the thickness of the SiC slab and the volume of the Mg atoms with the density at the simulation temperature.[3] In this way, we obtained a supercell with $a = 15.53$ Å and $c = 57.37$ Å for the Mg(*l*)/SiC{0 0 0 1} interfaces. The SiC substrate contains a Si-terminated and a C-terminated surface. This supercell contains in total 600 atoms: 100 Si, 100C and 400 Mg atoms. The supercell is deliberately large to obtain statistically meaningful results and to avoid risk of artificial crystallization in the liquid metal.

We employed a plane-wave pseudo-potential approach implanted into the first-principles package VASP (Vienna *Ab initio* Simulation Package).[37] This code uses the first-principles density functional theory (DFT) within the projector-augmented wave (PAW) framework.[38] The generalized gradient approximation has been employed to describe the exchange and correlation terms.[39] The cut-off energies used are $E_{CUT}/E_{AUG} = 450.0$ eV/650.0 eV which are higher than the default values of the atoms ($E_{MAX}/E_{AUG} =$ 245.3 eV/322.1 eV for Si, 400.0 eV/644.9 eV for C and 200.0 eV/454.7 eV for Mg, respectively). The higher cu-off energies describe the atomic behavior solid better and may provide more reliable results.[37]

For the AIMD simulations, we employed a cut-off energy of 320 eV which is higher than the E_{MIN} values of the pseudopotentials of the related atoms, and the Γ-point in the Brillouin zone (BZ).[40] The latter is due to the lack of periodicity of the whole Mg(*l*)/SiC systems.[15,23,41] Such settings help balance the computational costs and reliability of the results. Test simulations from 200 to 400 eV showed the present cut-off energy is reasonable.

We prepared liquid Mg samples by equilibrating for about 6 ps at 3000 K. Then, the prepared samples were cooled to the designed temperature to eliminate excess internal stress and defects created at the high-temperature. The obtained liquid Mg samples together with the SiC{0 0 0 1} slab were used for building the Mg(*l*)/SiC{0 0 0 1} systems. A two-step approach was employed for equilibrating the Mg(*l*)/SiC{0 0 0 1} systems: AIMD simulations were first performed with the substrate atoms pinned for 3 ps (1.5 fs per step). Then, we equilibrated further the systems with full relaxation of the atoms for another 4000 steps. Analysis showed no further changes of atomic ordering at the interfaces. The two-step approach avoids risk of possible collective atomic movements occurring when we relax all atoms from start as shown in the previous simulations.[22,23] The time-averaged method was used to sample the interfaces over 3.0 ps to ensure statistically meaningful results. This approach has been widely used in *ab initio* molecular dynamics simulations for liquid–metal/solid-metal interfaces[15,23] and other liquid–metal/solid-substrate interfaces.[41,42]

III. RESULTS

The calculated results for the solid components, α-Mg, 4H-SiC and 6H-SiC are presented first. These compounds have hexagonal lattices as shown in the literature.[3,5,18–20] The calculated lattice parameters are at ambient conditions (0 K and 0 Pa). The calculated lattice parameters are $a = 3.193$ Å, $c = 5.178$ Å (experimental values $a = 3.209$ Å, $c = 5.210$ Å at room temperature[3]) for α-Mg; $a = 3.093$ Å, $c = 10.127$ Å (experimental values: $a = 3.0805$ Å, $c = 10.085$ Å[43]) for 4H-SiC; and $a = 3.094$ Å, $c = 15.182$ Å (experimental values $a = 3.081$ Å, $c = 15.117$ Å[44]) for 6H-SiC. The calculated lattice parameters are in good agreements with the experimental observations with deviations within 1 pct. Moreover, the calculations revealed close formation energies for 4H- and 6H-SiC, in agreement with the experimental observations that these two forms of SiC occur frequently.[18–20]

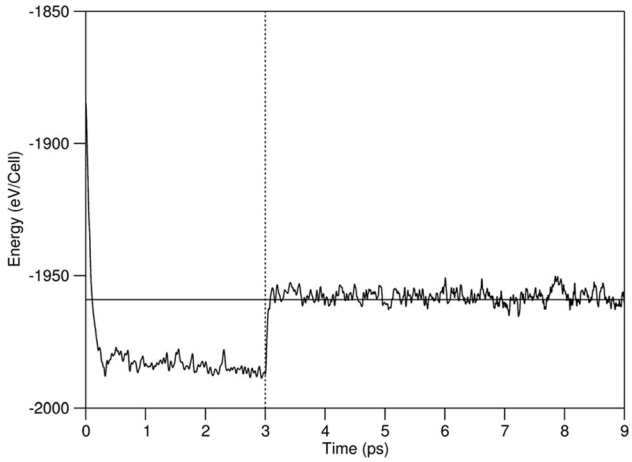

Fig. 1—Relation between the total valence-electron energy of the Mg(*l*)/SiC{0 0 0 1} system and simulation time at 1000 K. The vertical dotted line represents the border between Step 1 with pinned substrate atoms and Step 2 with all atoms relaxed.

We turn here to the AIMD simulations for the Mg(*l*)/SiC{0 0 0 1} interfaces at 1000 K. During the simulations, the nearby liquid Mg atoms move towards the SiC substrates and gradually form stable layers nearby the substrates. Correspondingly, the total valence-electron energy of the system decreases quickly at first 0.5 ps (Figure 1). Then, it stabilizes and oscillates with simulation time. Releasing of the pinned atoms raises the energy due to the movements of the substrate atoms. The system reached equilibrium again within 1 ps.

A snapshot of the equilibrated Mg(*l*)/SiC{0 0 0 1} interfaces is shown in Figure 2(a). The atomic arrangements of the outmost SiC double-atom layer and terminating Mg atoms are shown at the Si-terminated (S2) in Figure 2(b) and at the C-terminated (S1) interface in Figure 2(c), respectively.

The Si and C atoms at the substrates are well ordered, corresponding to the high stability of SiC. Meanwhile, the Mg atoms away from the interfaces exhibit no apparent long-range ordering and are liquid-like. The liquid Mg atoms adjacent to the SiC substrates exhibit both atomic ordering and density variation along the orientation perpendicular to the substrate. The latter is referred to as atomic layering.[14,15,45]

Atomic density profile at the interface along the orientation perpendicular to the substrate, $\rho(z)$ is defined as[14,45]:

$$\rho(\mathrm{z}) \;=\; < N_{\mathrm{z}}(t) > / \left(L_{\mathrm{x}} L_{\mathrm{y}} \Delta z \right) \qquad [1]$$

Here, L_{x} and L_{y} are the in-plane x and y dimensions of the unit cell, respectively, and z the dimension perpendicular the substrate. Δz is the bin width, and $N_{\mathrm{z}}(t)$ is the number of atoms between $z - (\Delta z/2)$ and $z + (\Delta z/2)$ at time t. $< N_{\mathrm{z}}(t) >$ represents a time-averaged number of atoms in the duration. The unit of $\rho(z)$ is ($\mathrm{\AA}^{-3}$). We assess the layering phenomena at the interfaces using the atomic density profile which using Eq. [1]. The obtained atomic density profiles for the atoms at the C-terminated and Si-terminated Mg(*l*)/SiC{0 0 0 1} interfaces are shown in Figure 3.

Figure 3 shows sharp peaks in the substrates. This corresponds to the ordered substrate Si and C atoms in Figure 2(a). The liquid-like Mg atoms away from the substrates form little variation at the density profiles. Figure 3 also shows strong layering in the liquid Mg adjacent to the substrates. There are also subtle differences for the Mg atoms near the C-terminated and Si-terminated interfaces. Correspondingly, the chemical bonding is notably different as shown in Figure 2(c) for the interfacial C-Mg bonds, at which the terminating Mg atoms are positioned dominantly at the top of C-triangles and in Figure 2(b) for the interfacial Si–Mg bonds.

There are five recognizable Mg layers (including the terminating Mg layer) at the C-terminated and six at the Si-terminated interfaces (Figure 3). These numbers are as high as those of the Al(l)/Al(s) interfaces without lattice misfit (six atomic layers).[14,15] Thus, the layering phenomenon at the Mg(*l*)/SiC{0 0 0 1} interfaces is unusually strong.

The heights of the liquid Mg layers decrease with increasing distances from the substrate-surfaces. The terminating Mg layer at the C-terminated interfaces has a peak higher than that at the Si-terminated interface. The terminating Mg layers at both interfaces are well separated from the substrates and have little mixing with the 1st Mg layers. Meanwhile, the Mg atoms at the 1st layers are mixed with those of the 2nd layers. From the 2nd Mg layer, all the Mg layers are mixing with the neighboring layers. The distance between the C peak to the Mg peak is 1.7 Å, notably shorter than that between the terminating Mg and the outmost Si layer (2.4 Å). The interpeak distances between the rest Mg layers are about 2.6 Å, close to the atomic spacing along the Mg{0 0 0 1} orientation.

We analyzed the number of atoms at the interfacial layers using the term occupation rate that is defined as the number of Mg atoms at a Mg layer n(Mg) in the unit area divided by the number of Si/C atoms $n(X)$ per aera with X = Si or C at a substrate layer for configurations over 3 ps in the AIMD simulations. That is, n(Mg)/$n(X)$ with X = Si or C. The obtained atom's occupation ratios are: n(Mg)/n(C) = 0.949 for the terminating Mg layer, 0.852 for the 1st and 0.831 for the 2nd Mg layer at the C-terminated interface; n(Mg)/n(Si) = 0.838 for the terminating Mg layer, 0.851 for the 1st and 0.835 for the 2nd Mg layer at the Si-terminated interface. The ratios between the Mg atoms to that of the substrate atoms are smaller than 1.0, corresponding to the larger atomic size of Mg than those of Si or C. For the terminating Mg layers, the n(Mg)/n(C) ratio is higher than the n(Mg)/n(Si) at the Si-terminated interface. This comes from stronger C-Mg bonding than Si–Mg (Figure 2), which will be addressed later.

The epitaxial nucleation model suggested a layer-by-layer growth for a solid phase at a substrate in liquid.[46] The atomic ordering of the Mg layers nearby the substrates plays a crucial role during solidification. Therefore, we analyzed the atomic arrangements of the layers nearby the substrates for the equilibrated

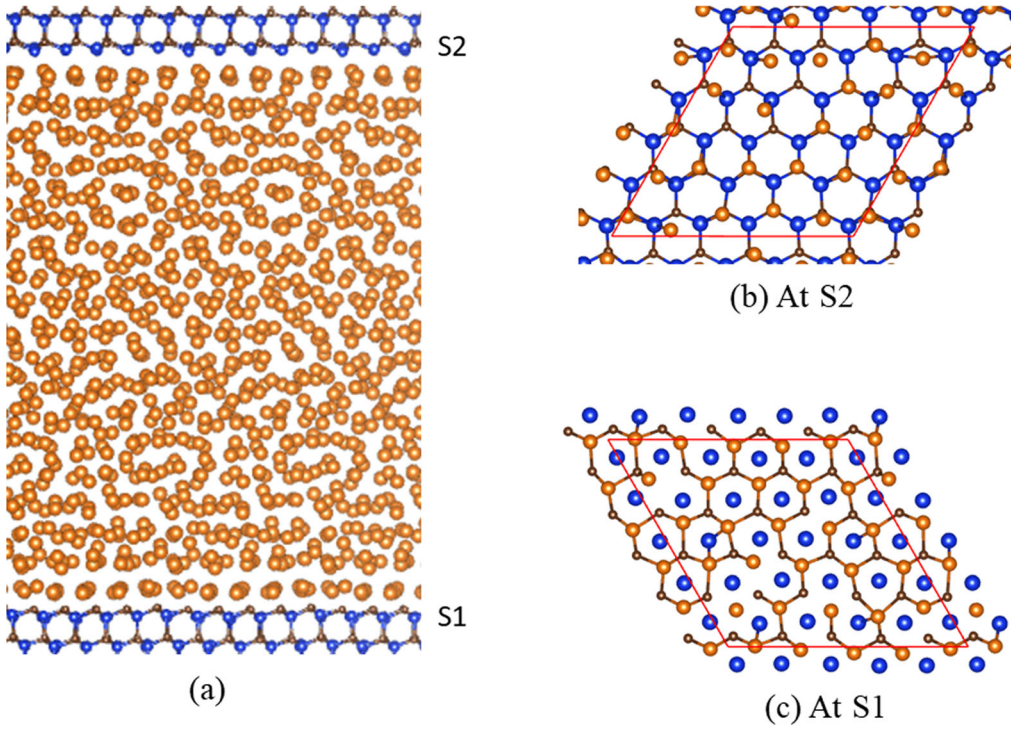

Fig. 2—A snapshot of the equilibrated Mg(*l*)/SiC{0 0 0 1} interfaces (*a*) and the related interfacial bonding at the C-terminated S1 (*c*) and at the Si-terminated S2 (*b*). The orange spheres represent Mg, small dark-brown C and blue Si. The labels S1 and S2 in Fig. 1(a) represent for the C-terminated and Si-terminated interface, respectively (Color figure online).

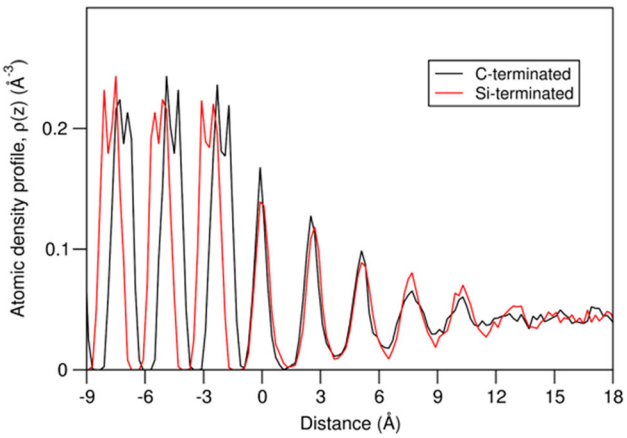

Fig. 3—The atomic density profile, $\rho(z)$ of the equilibrated Mg(*l*)/SiC{0 0 0 1} interfaces at 1000 K. We set the peaks of the terminating Mg layers at zero Å at *x*-axis (Color figure online).

configurations over 3 ps, which are shown in Figures 4(a) through (d) for the C-terminated interface and Figures 4(e) through (h) for the Si-terminated interface. Moreover, we also assess the ordering of the Mg atoms at each layer using the in-plane atomic ordering coefficients[45] for the averaged configurations. The obtained results are plotted in Figure 5.

Figures 4 and 5 show that the outmost C (Figure 4(a)) and Si (Figure 4(e)) atoms exhibits well-ordering and strong localized nature. Correspondingly, their in-plane atomic ordering coefficients are as high as those in the inner part ($S(z) \sim 0.90$). The terminating Mg atoms at the C-terminated interface exhibit pronounced ordering and strongly localized nature with $S(z) \sim 0.45$, whereas the terminating Mg atoms at the Si-terminated interface show weak ordering and delocalized nature ($S(z) \sim 0.10$). The Mg atoms at the 1st Mg layer at both interfaces exhibit little ordering and delocalized nature with $S(z) < 0.05$ (Figure 5). The Mg atoms at the 2nd Mg layer at both interfaces exhibit more liquid-like.

Overall, the in-plane atomic ordering at the Mg(*l*)/SiC{0 0 0 1} interfaces is weak, which is in contrast to the strong layering phenomena. The in-plane ordering of the terminating Mg layer at the C-terminating interface is notably stronger than that the Si-terminating interface, whereas the layering at the latter is higher than the latter. The observed phenomenon relates to interfacial interactions.

To get insight into the unusual prenucleation at the interfaces, we performed first-principles electronic structure calculations for an equilibrated Mg(*l*)/SiC{0 0 0 1} system. The obtained electron density distributions are shown in Figure 6(a). The partial density of states (pDOS) for the selected atoms are shown in Figure 7.

Figure 6(a) shown low density distributions around the Mg ions, corresponding to its free electron nature. The calculated pDOS curves also showed little occupied state at the valence bands for the Mg atoms (Figures 7(e) through (h)). Meanwhile, high densities of electrons around the Si and C atoms, which indicates the strong bonding between Si and C in the substrates. This is reflected in the high pDOS in Figures 7(a) through (d). Figures 7(b) and (c) also showed a band

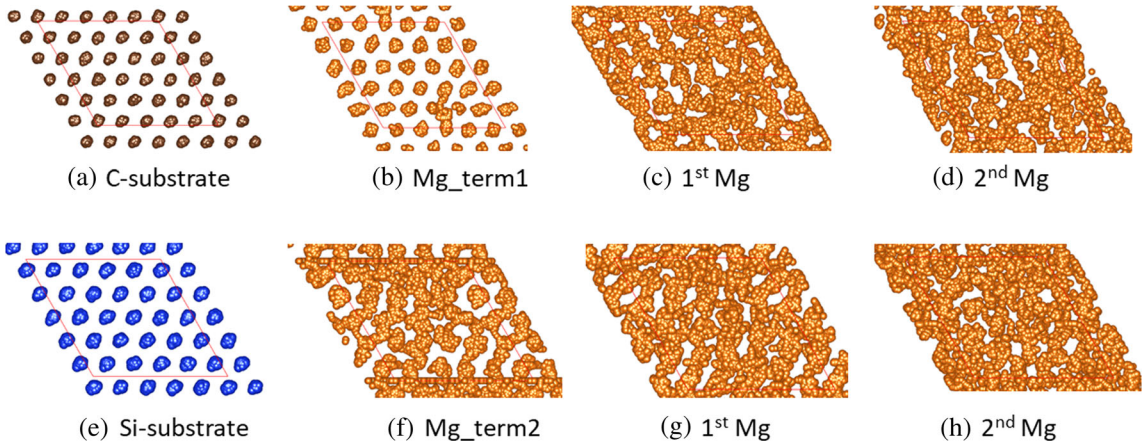

Fig. 4—Atomic arrangements of the outmost substrate C layer (*a*) and Si layer (*e*) and the corresponding terminating Mg layers (*b*, *f*), 1st Mg layers (*c*, *g*) and 2nd Mg layers (*d*, *h*), respectively. The meaning of the spheres is the same as that in Fig. 2 (Color figure online).

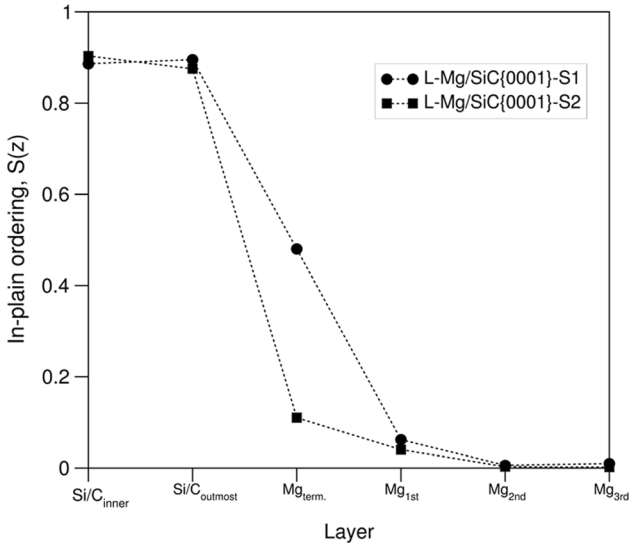

Fig. 5—Atomic in-plane ordering coefficients of the substrate layers and the Mg layers at the two interfaces. The dotted lines connecting the values are used to guide readers' eyes. S1 represents the C-terminated and S2 the Si-terminated interface, respectively (See Fig. 2).

gap ~ 2.0 eV for the Si and C atoms in the substrate slab. Tails of density of states from the nearby Mg atoms fall into the gap of the interfacial Si and C atoms (Figures 7(a) and (d)).

In order to have direct knowledge of the chemical interaction at the Mg(*l*)/SiC{0 0 0 1} interfaces, we employed the Bader's charge model[47,48] implanted into VASP.[49] The obtained results are shown in Figure 6(b).

In the substrate the C atoms obtain about 1.5 e/C electrons, being $Si^{+1.5}C^{-1.5}$ (Figure 6(b)). Such charge transfer agrees with the large difference of their electronegativity values. However, the amount of charge transfer is far smaller than those in the ionic model, indicating strong covalence between Si and C. The Mg atoms away from the substrates are electronically neutral. The Mg atoms adjacent to the substrates loss electrons and become positive charged, with + 0.5 e/Mg at the C-terminated interfaces and 0.2 e/Mg at the Si-terminated interface. This corresponds to the lower electronegative value of Mg (1.31) as compared with those of C and Si.

IV. DISCUSSIONS

Prenucleation at a liquid/solid interface provides a precursor for following nucleation, and thus it relates to the intrinsic capability (potency) of the substrate to nucleate the solid.[16] At a temperature above the nucleation point, prenucleation at a solid/liquid interface is determined by four factors, the temperature,[15] the lattice misfit between the substrate and the metal, *f*,[14,16] interfacial chemical interaction[15] and atomic roughness of the substrate, *R* which is defined as[22,50–52]:

$$R = \left[\sum |\Delta z(i)|/d_0\right]/N_z \times 100, \qquad [2]$$

where Δz(i) is the deviation of atom i from the atomic line, d_0 is the atomic spacing in the *z*-direction, and N_z is the atoms in unit cell of the layer. The unit of atomic roughness is pct. $R = 0$ means all atoms being positioned at the line of the layer.

The interfacial interaction can be rated by charge transfer at the interfaces.[52] The present calculations provide an opportunity to discuss the influences of these factors of the substrates on prenucleation in liquid Mg. We compare the results of the Mg(*l*)/SiC interfaces and those of the Mg(*l*)/Zr[51] and Mg(*l*)/MgO[22] interfaces in the literature in Table I.

Both Zr and Mg have a hcp close-packed structure.[51] The lattice mismatch between Zr{0 0 0 1} and Mg is minor (< 1.0 pct).[3,51] The electronegativity difference between the two elements is also small (1.31 for Mg *vs* 1.33 for Zr in Pauling scale). These properties are reflected in the results of the AIMD simulations.[51] The terminating Mg atoms form a flat layer with full occupation. The interfacial charge transfer is ignorable (Table I). Strong prenucleation occurs at the Mg(*l*)/Zr{0 0 0 1} interface. There are seven recognizable liquid

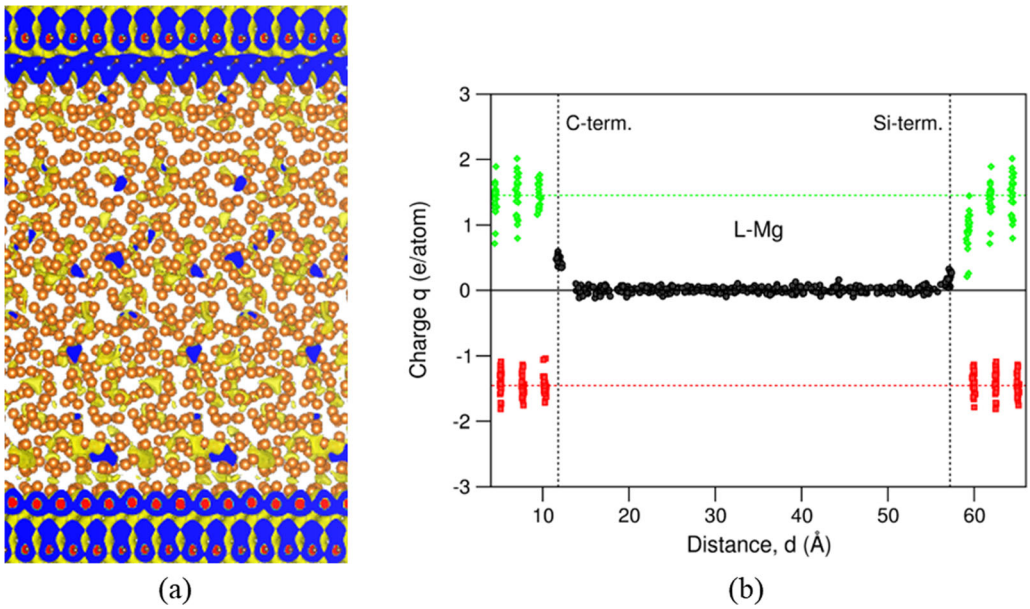

Fig. 6—(*a*) Iso-surfaces of electron density distributions ($\rho_0(r)$ = 0.019e/Å^3) and (*b*) the Bader charges at the Mg(*l*)/SiC{0 0 0 1} interfaces (Color figure online).

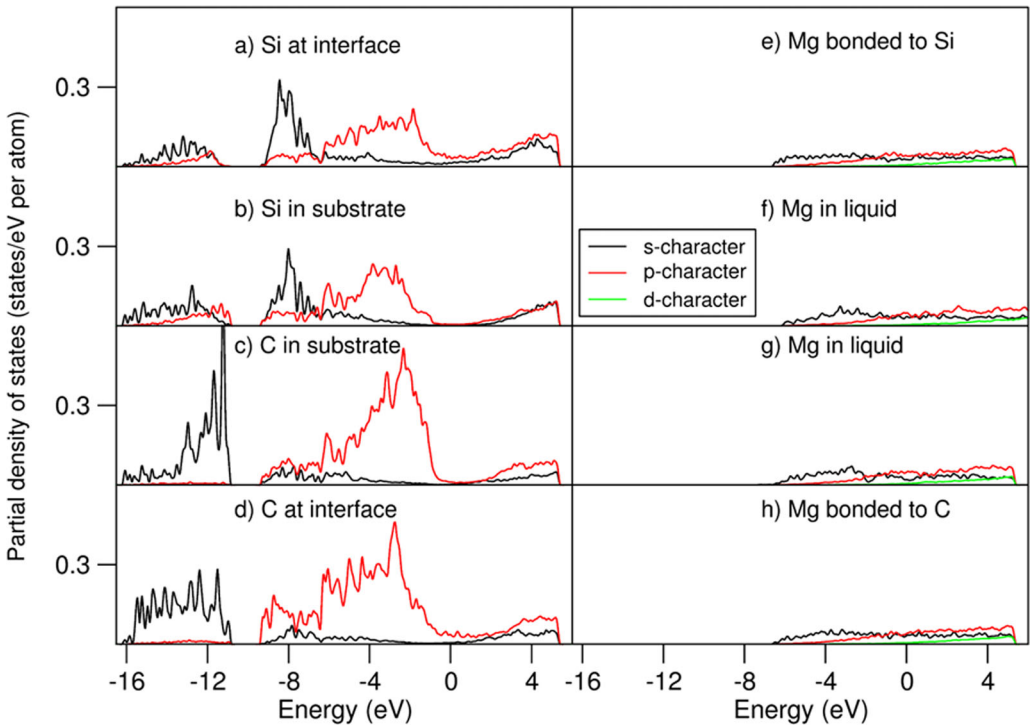

Fig. 7—Partial density of states (pDOS) of selected atoms in the Mg(*l*)/SiC{0 0 0 1} interface systems. The Fermi level is at zero eV. The black curves represent the s-characters, red p-characters. Partial density of states of (*a*) an interfacial Si atom, (*b*) one Si atom in the substrate, (*c*) an interfacial C, (*d*) one C in the substrate; (*e*) an interfacial Mg atom bonded to Si, (*f*) one Mg atom away from the interfaces, (*g*) one Mg atom in the liquid and (*h*) an interfacial Mg bonded to C (Color figure online).

layers. The in-plane ordering coefficient for the terminating Mg layer is 0.42. Such pronounced prenucleation at the Mg(*l*)/Zr{0 0 0 1} interface is similar to the idealized model, the liquid-Al/Al{1 1 1} interfaces.[14,15] The simulated results agree with the fact that up to now Zr is the widely used grain-refiner in industry for casting of Mg metals/alloys.[16,51–53]

Table I. List of the Lattice Misfits Between the Substrates and the Light Metals, Substrates Surface Features Including Atomic Roughness *R via* Eq. [2], and Prenucleation (Number of Ordered Layers, n_{Layers}, In-Plane-Ordering of the Terminating Metal Layers, $S_M(z)$) for Mg(*l*)/SiC{0 0 0 1} (This Work), Mg(*l*)/MgO{1 1 1}[22,51,52]; and Mg(*l*)/Zr{0 0 0 1}[22,51]

Interface	*f* (Pct)	M Oc. (Pct)	*R* (Pct)	*q*(e/Mg)	n_{Layers}	$S_M(z)$	Prenucl
Mg(*l*)/Zr{0 0 0 1} [51]	+ 0.7	100	0.0	0.02e	7	0.42	Strong layering Strong in-plane ordering
Mg(*l*)/SiC{0 0 0 1}$_C$ (This work)	+ 5.9	95	2.5	+ 0.50	5	0.45	Strong layering Weak in-plane ordering
Mg(*l*)/SiC{0 0 0 1}$_{Si}$ (This work)		85	7.5	+ 0.21	6	0.10	Strong layering Weak in-plane ordering
Mg(*l*)/MgO{111}$_{Mg}$[22,51–53]	+ 7.9	92	4.0	+ 0.60	3–4	0.01	Moderate layering Weak in-plane ordering

The opposite example is the interface between Mg(*l*)/MgO{1 1 1).[22,51,53] As shown in Table I, the misfit between Mg{0 0 0 1} and MgO{1 1 1} is large (7.9 pct). The AIMD simulations revealed that the terminating Mg atoms at the Mg(*l*)/MgO{1 1 1} interface form a flat layer with vacancies at the terminating Mg layer.[22,51] The formation of such vacancies is corresponding to the lattice mismatch (Table I) that the surface area is too small to host full occupation of Mg atoms.[22,51] Such atomic vacancies can be treated as atomic roughness at the substrate surface. Charge transfer at the interface is 0.6 e/Mg on average.[22,51] The simulations revealed moderate layering and weak in-plane ordering at the interface. This confirmed the previous studies that lattice misfit has little influences on layering but strong on in-plane-ordering, and atomic roughness reduces both layering and in-plane ordering.[50,51,53]

The lattice misfit between SiC{0 0 0 1} and Mg{0 0 0 1} is also notable (5.9 pct). The terminating Mg layers are flat. There are moderate interfacial charge transfers (Table I). There are vacancies at the terminating Mg layers and thus, the SiC{0 0 0 1} substrate-surfaces are atomically rough. Prenucleation at the Mg(*l*)/SiC{0 0 0 1} interfaces shows complex behaviors. The Si-terminated interface has more pronounced layering but weaker in-plane ordering than the C-terminated interface. This corresponds well to the severer atomic roughness causes by vacancies at the former (Table I). It is also notable that the in-plane ordering coefficient at the terminating Mg layer at the C-terminated interface is higher than that at the Mg(*l*)/Zr{0 0 0 1}, which originates from the stronger C-Mg bonding and the strong Si–C covalent bonding in the substrate (melting temperature for SiC is 2830 °C, notably higher than that of Zr, 1855 °C).

The present AIMD simulations revealed mixed behavior of prenucleation at the Mg(*l*)/SiC{0 0 0 1} interfaces. Comparatively, prenucleation at the Mg(*l*)/SiC{0 0 0 1} interfaces is more significant than that at the Mg(*l*)/MgO{1 1 1} interfaces as shown in Table I. This indicates that if there are no significant amount of more potent substrates, such as Zr in the Mg liquid, the added SiC particles of significance may act as potential nucleation sites, meanwhile the newly formed MgO particles during the casting play a less important role as potential nucleation sites during casting if there is a significant amount of SiC particles existing in the liquid.[16,22,51,52] The obtained information here is helpful to get insight into the interaction between liquid magnesium and SiC during the preparation of nano-MMCs,[6,7] but also for developments of new grain refiners for Mg,[3,11,53,54] and further to understand the solidification of light metals[13,16,17] in general.

V. SUMMARY

We performed *ab initio* molecular dynamics simulations for the interfaces between liquid Mg and SiC{0 0 0 1} substrates. This study revealed the following results.

(i) There are distinct borders between the substrates and liquid Mg at the Mg(*l*)/SiC{0 0 0 1} interfaces.
(ii) The Mg layers adjacent to the SiC substrates are flat with atomic vacancies, being topologically rough.
(iii) There are moderate charge transfers from the Mg atoms to the outmost C (0.5 e/Mg) and Si atoms (0.2 e/Mg), respectively.
(iv) The in-plane ordering at the C-terminated interface is more pronounced than that at the Si-terminated interface, corresponding to the stronger interfacial C-Mg interaction.
(v) Unusual prenucleation occurs at the Mg(*l*)/SiC{0 0 0 1} interfaces. There is pronounced layering (five to six recognized layers) but faint in-plane ordering.

The obtained information here helps understand the interactions between liquid Mg and SiC particles and the role of SiC particles in nucleation of Mg metals. Furthermore, it is useful to get insight into the stability of the (nano-)MMCs and further to design new MMCs of fine and uniform microstructures and desirable properties.

ACKNOWLEDGMENTS

Financial support from EPSRC (UK) under Grant number EP/N007638/1 and EP/V011804/1 is gratefully acknowledged.

CONFLICT OF INTEREST

The authors declare that they have no competing interest.

OPEN ACCESS

REFERENCES

1. Handbook Committee, *Properties and Selection: Nonferrous Alloys and Special-Purpose Materials*, Metal Handbook, Vol. 2, ASM International, Materials Park, 1990.
2. W.J. Joost: *Magnesium Technology*, Wiley, New York, 2014.
3. J.W. Arblaster: *Selected Values of the Crystallographic Properties of the Elements*, ASM International, Materials Park, 2018.
4. J.F. Song, J. She, D.L. Chen, and F.S. Pan: *J. Mag. Alloys*, 2020, vol. 8, pp. 1–41.
5. R.W.G. Wyckoff: *The Structure of Crystals*, 2nd ed. Reinhold Publishing Corporation, New York, 1935.
6. H.Z. Ye and X.Y. Liu: *J. Mater. Sci.*, 2004, vol. 39, pp. 6153–71.
7. R. Saranu, R. Chanamala and S. Putti, in *2020 IOP Conf. Ser.: Mater. Sci. Eng.*, 2020, vol. 961, p. 012001.
8. J. Leito, P.L. Zak, A.A. Shirzadi, A.L. Greer, W.K. Krajewsli, J.S. Suchy, K. Haberl, and P. Schumacher: *Acta Mater.*, 2012, vol. 60, pp. 2950–58.
9. M. Gupta, M.O. Lai, and D. Saravanaranganathan: *J. Mater. Sci.*, 2000, vol. 35, pp. 2155–65.
10. L.-Y. Chen, J.-Q. Xu, H. Choi, M. Pozuelo, X.L. Ma, S. Bhowmick, J.-M. Yang, S. Mathaudhu, and X.-C. Li: *Nature*, 2015, vol. 528, pp. 539–43.
11. Y. Cai, D. Taplin, M.J. Tan, and W. Zhou: *Scr. Mat.*, 1999, vol. 41, pp. 967–71.
12. E. Karakulak: *J. Mag. alloys*, 2019, vol. 7, pp. 355–69.
13. Y. Cai, M.J. Tan, G.J. Shen, and H.Q. Su: *Mater. Sci. Eng. A*, 2000, vol. 282, pp. 232–39.
14. H. Men and Z. Fan: *Metall. Mater. Trans.*, 2018, vol. 49A, pp. 2766–77.
15. C.M. Fang, H. Men, and Z. Fan: *Metall. Mater. Trans.*, 2018, vol. 49A, pp. 6231–42.
16. Z. Fan, in *The 11th International Conference on Magnesium Alloys and Their Applications*, 24–27 July 2018, Beaumont Estate, Old Windsor, UK. ed. by Z. Fan and C. Mendis, 2018, p. 7.
17. Z. Fan, G. Gao, B. Jiang, and Z.P. Que: *Sci. Rep.*, 2020, vol. 10, p. 9448.
18. R. Willardson and E.R. Weber: *SiC Materials and Devices*, Academic Press, New York, 1998, pp. 1–18.
19. M.R. Katkova, S.S. Nosov, M.A. Faddeev, and E.V. Chuprunov: *Cryst. Rep.*, 1999, vol. 44, pp. 795–98.
20. F. Kelly, G.R. Fisher, and P. Barnes: *Mater. Res. Bul.*, 2005, vol. 40, pp. 249–55.
21. P.W. Tasker: *Philos. Mag.*, 1979, vol. 39A, pp. 119–36.
22. C.M. Fang and Z. Fan: *Metall. Mater. Trans.*, 2020, vol. 51A, pp. 788–97.
23. C.M. Fang and Z. Fan: *Metall. Mater. Trans.*, 2022, vol. 53A, pp. 2040–47.
24. M.S. Yaghmaee and G. Kaptay: *Mater. Sci. Forum*, 2005, vol. 473–474, pp. 415–20.
25. S. Kamrani, D. Penther, A. Ghasemi, R. Riedel, and C. Fleck: *Adv. Powder Technol.*, 2018, vol. 29, pp. 1742–48.
26. X. Zhou, W.M. Bu, S.Y. Song, F. Sansoz, and X.R. Huang: *Mater. Des.*, 2019, vol. 182, p. 108093.
27. X.L. Yang, F. Wang, and Z.Y. Fan: *J. Alloys Compds.*, 2017, vol. 706, pp. 430–37.
28. W.R.L. Lambrecht, S. Limpijumnong, S.N. Rashkeev, and B. Segall: *Phys. State. Sol. B*, 1997, vol. 202, pp. 5–33.
29. G. Cicero and A. Catellani: *Chem. Phys.*, 2005, vol. 122, p. 214716.
30. S. Li, R.J. Arsenault, and P. Jena: *J. Appl. Phys.*, 1988, vol. 64, pp. 6246–53.
31. C.Q. Wang, W.G. Chen, and J.P. Xie: *Metals*, 2020, vol. 10, p. 1197.
32. X.Y. Xu, H.Y. Wang, M. Zha, C. Wang, Z.Z. Yang, and Q.C. Jiang: *Appl. Surf. Sci.*, 2018, vol. 437, pp. 103–09.
33. A.-H. Zou, X.-J. Zhou, Z.-B. Kang, Y.-H. Rao, and K.-Y. Wu: *J. Inorg. Mater.*, 2019, vol. 34, pp. 1167–74.
34. B.B. Liu and J.F. Yang: *J. Alloys Compds.*, 2019, vol. 791, pp. 530–39.
35. J. Li, M. Zhang, J.Y. Zhao, Y.M. Cui, and X. Luo: *Appl. Surf. Sci.*, 2020, vol. 511, p. 145633.
36. D.N. Talwar and J.C. Sherbondy: *Appl. Phys. Lett.*, 1995, vol. 67, pp. 3301–03.
37. G. Kresse and J. Furthmüller: *Comput. Mater. Sci.*, 1996, vol. 6, pp. 15–50.
38. P.E. Blőchl: *Phys. Rev. B*, 1994, vol. 50, pp. 17953–78.
39. J.P. Perdew, K. Burke, and M. Ernzerhof: *Phys. Rev. Lett.*, 1996, vol. 77, pp. 3865–68.
40. H.J. Monkhorst and J.D. Pack: *Phys. Rev. B*, 1976, vol. 13, pp. 5188–92.
41. W. Brostow and H.E. Hagg Lodbland: *Materials: Introduction and Applications*, Wiley, Hoboken, 2017.
42. L.E. Hintzsche, C.M. Fang, T. Watts, M. Marsman, G. Jordan, G.M.W.P.E. Lamers, A.W. Weeber, and G. Kresse: *Phys. Rev. B*, 2012, vol. 86, p. 235204.
43. N.W. Thibault: *Am. Miner.*, 1944, vol. 29, pp. 249–78.
44. G.C. Capitani, G. Tempesta, S. Di Pierro, and E. Scandale: *Acta Cryst.*, 1967, vol. 62A, p. s200.
45. A. Hashibon, J. Adler, M.W. Finnis, and W.D. Kaplan: *Comput. Mater. Sci.*, 2002, vol. 24, pp. 443–52.
46. Z. Fan: *Metall. Mater. Trans.*, 2013, vol. 44A, pp. 1409–18.
47. R.F.W.A. Bader: *Chem. Rev.*, 1991, vol. 91, pp. 893–928.
48. R.F.W. Bader: *J. Phys. Chem. A*, 1998, vol. 102, pp. 7314–23.
49. G. Henkelman, A. Arnaldsson, and H. Jónsson: *Comput. Mater. Sci.*, 2006, vol. 36, pp. 254–360.
50. B. Jiang, H. Men, and Z. Fan: *Comput. Mater. Sci.*, 2018, vol. 153, pp. 73–81.
51. C. M. Fang and Z. Fan, in *Proc. The 11th International Conference on Magnesium Alloys and Their Applications*, 24–27 July 2018, Beaumont Estate, Old Windsor, UK. ed. by Z. Fan and C. Mendis, 2018, pp. 41–50.
52. Z. Fan, F. Gao, Y. Wang, S.H. Wang, and J.B. Patel: *J. Magn. Alloys*, 2022, vol. 10, pp. 2919–45.
53. C.M. Fang and Z. Fan: *Metals*, 2022, vol. 12, p. 1618.
54. Y. Ali, D. Qiu, B. Jiang, F.S. Pan, and M.-X. Zhang: *J. Alloys Compds.*, 2015, vol. 619, pp. 639–51.